13^{th} Congress of Intl. Maritime Assoc. of Mediterranean
IMAM 2009, Istanbul, Turkey, 12-15 Oct. 2009

On the Influence of the Water Depth on Wave-Structure-Interactions

G. Clauss, F. Stempinski, M. Dudek, M. Klein
Technical University Berlin, Naval Architecture & Ocean Engineering, Berin, Germany

ABSTRACT: For seakeeping model tests and the experimental investigation of offshore operations the water depth is a parameter which is difficult to adjust to a particular problem and scale, especially in small testing facilities. Therefore, it is desirable to violate or ignore the condition "water depth" and to use larger models minimizing scaling effects. In this paper its influence is examined in order to clarify how it affects wave kinematics, wave forces, and seakeeping, and where the deep water assumption holds.
After a short recapitulation of the water wave theory, a freak wave sequence is presented being reproduced at two different wave tanks at scales 1:75 and 1:81 and investigated analytically. The comparison of the wave kinematics reveals that moderate water depths are of minor importance for extreme waves with identical surface elevations but different water depths.
In order to examine the effects regarding wave structure interaction model tests are conducted at various water depths using the huge semi-submersible crane vessel Thialf. The model tests are accompanied by numerical calculations utilizing the panel code WAMIT. It is shown that for the given scale of 1:75 a water depth of 1 m is sufficient to model deep water conditions.

1 INTRODUCTION

Since the water depth is often the least adjustable parameter in model testing it governs the scale at which experiments are conducted. Especially in shallow basins this may lead to large model scales where other scale effects, e.g. viscosity related effects, have detrimental effects on the significance of the results. Therefore, it is often desirable to violate or ignore the condition "water depth" and to use larger models and conduct model tests at higher Reynolds numbers. Additionally, the handling and installation effort in the experimental procedures can be reduced significantly, if the floating model is accessible by a person standing in the water.

The question whether the benefit outweighs the error is the scope of the following considerations. To gain a clear understanding the problem is approached in two stages: First the influence of the water depth on the water waves – especially the particle kinematics which are the primary causation of the structure motions – is presented. A deterministic wave sequence, the well known New Year Wave, is presented being realized in two wave tanks at scale 1:70 and at scale 1:81 (Clauss et al. (2008a), Clauss et al. (2007)). Both data sets represent the same wave group in time and space and are reproduced in two testing facilities at two different relative water depths.

The next step is to assess the wave structure interaction focussing on the changes of the hydrodynamic coefficients in seakeeping when the water depth decreases. Effects related to water depth are well known in resistance and maneuvering tests. The crane-semi-submersible Thialf has been chosen for assessing the influence of the water depth on heave and pitch motion. In previous investigations by Riekert (1992) a motion analysis of the vessel with and without hanging loads is conducted. Jacobsen and Clauss (2005) investigated the seakeeping behavior in detail in time and frequency domain deriving definitions of operational limits and the coupling effects with a barge floating nearby. All model tests have been conducted at water depths of more than 100 m (large scale) while in the theory deep water is assumed. In this paper a series of model tests and calculations is presented in which the motion behavior of the crane-semi-submersible Thialf is investigated focussing on the effect of the water depth on the hydrodynamic coefficients i.e. potential damping, added mass and exciting forces.

2 REVIEW OF WAVE THEORY

The influence of limited water depth d is induced by the presence of the bottom boundary condition. The origin of the coordinate system ($z = 0$) is set to the mean water line and the sea bottom is assumed to be flat, rigid, and impermeable. With ϕ being the flow potential and w the

vertical velocity the bottom boundary condition is

$$w(z=-d)=\frac{\partial\phi}{\partial z}=0. \tag{1}$$

It causes the particle trajectories to become elliptical which is mathematically expressed by the hyperbolic decay terms D_h, D_v valid for displacement, velocities, and accelerations which are for all horizontal particle dynamics:

$$D_h=\frac{\cosh(k(z+d))}{\sinh(kd)}$$

and for the respective vertical particle motion

$$D_v=\frac{\sinh(k(z+d))}{\sinh(kd)}$$

as illustrated in Fig. 1. Here, k denotes the wave number. The water depth can be neglected if it exceeds one half of the wave length $d/L=\omega^2 d/(2\pi g)<1/2$. At this depth the wave kinematics decay down to less than 5 per cent and are therefore negligible. The decay terms D_v and D_h can then be approximated by the general exponential function e^{kz}:

$$\cosh k(z+d)\approx\sinh k(z+d)\approx\frac{1}{2}e^{kz+kd}$$

$$\cosh kd\approx\sinh kd\approx\frac{1}{2}e^{kd}.$$

To apply this simplification to the irregular seaways it must be assured that also the low frequent parts of the spectrum fulfil this deep water condition. At the shallow water limit $kd<0.314$ the influence of the water depth on the celerity vanishes and the waves become non-dispersive. Here, the generation of deterministic wave sequences become infeasible and other wave models such as Stream Function Theory or Cnoidal Theory must be employed, which are not considered in this paper. All further derivations address the deep and transitional region where finite amplitude wave theory is valid.

It is apparent that the strongest effect, the vanishing of vertical particle motion, is observed close to the sea bottom whereas particle velocities at the water surface are least affected. It also shows that even for water depths $kd<\pi/2$ the influence of the particle kinematics at the water surface region remains almost identical to the generally assumed deep water case. The ratio of the increase of the decay term for horizontal dynamics D_h/e^{kz} and the decrease of the vertical dynamics $D_v/e^{kz}$is shown in Fig. 2. While at the surface $z=0$ m the vertical dynamics remain unaffected the effect increases with the water depth. At the deep water limit $d/L=0.5$ (where L is the wavelength) the deviation of horizontal and vertical

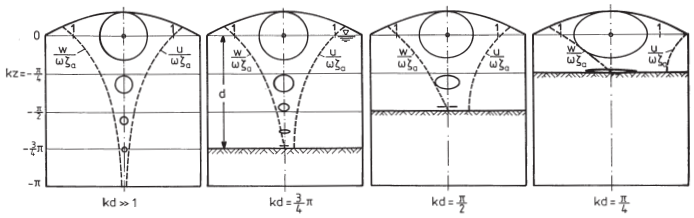

Figure 1: Deformation of orbital velocities depending on the relative water depth. The strongest effect i.e. the vanishing of vertical particle motion is observed close to the sea bottom whereas particle velocities at the water surface are least affected (Clauss et al. (1992)).

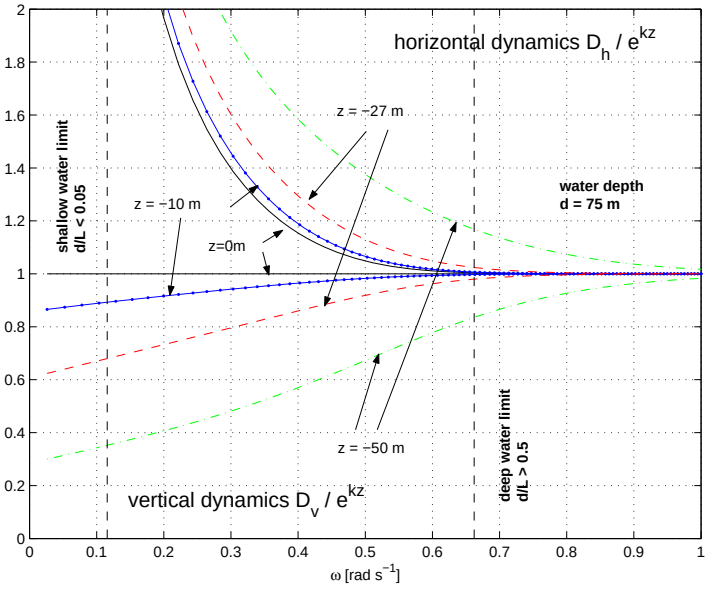

Figure 2: The ratio of increase of the decay term for horizontal dynamics D_h/e^{kz} and decrease of the vertical dynamics D_v/e^{kz} at distinct water depths.

motions lays at two per cent at $z=-27$ m which is the draft of the crane vessel. The dispersion relation (Stokes III)

$$\omega=\sqrt{kg\tanh kd\left(1+(\zeta_a k)^2\frac{\cosh 4kd+8}{8\sinh^4 kd}\right)} \tag{2}$$

and therefore the wave celerity and group velocity c_{gr} are affected:

$$c=\frac{\omega}{k}=\frac{L}{T} \tag{3}$$

$$c_{gr}=\frac{c}{2}\left[1+\frac{2kd}{\sinh 2kd}\right] \tag{4}$$

i.e. waves of one frequency become slower and shorter with decreasing water depth. The letter g denotes the gravity constant and is 9.81 m/s^2. From the fact that the energy flux in shallow water equals the one in deep water the steepening of the wave height can be derived as

$$\frac{H_{shallow}}{H_{deep}}=\sqrt{\frac{1}{\tanh(kd\left[1+\frac{2kd}{\sinh 2kd}\right]}}. \tag{5}$$

To conduct model tests with deterministic wave sequences the celerity is of great importance in order to realize an exact superposition pattern at a predefined location. Therefore, in Eq. 3 a higher order approach is utilized taking the finite amplitudes into account. The wave amplitudes must be adjusted according to Eq. 5 so that the desired surface elevation is achieved.

3 ANALYSIS OF DETERMINISTIC WAVE SEQUENCES AT VARIOUS WATER DEPTHS

For the investigation of the spatial development of an extreme sea state, the "New Year Wave", recorded at the Draupner platform in the North Sea on January 1^{st}, 1995, is chosen (Haver (2000)). This giant single wave ($H_{max} = 25.63\ m$) with a crest height of $\zeta_c = 18.5\ m$ occurred in a surrounding sea state characterized by a significant wave height of $H_s = 11.92\ m$ ($H_{max}/H_s = 2.15$). The water depth at the location is $d = 70\ m$. The wave group has been recovered in two different wave tanks. Each time the wave signal in time as well as the wave contour is recorded by successive measurements of a group of wave gauges that is shifted along the tank after each trial to yield the spatial development of the wave group. The specifics of the generation of this group

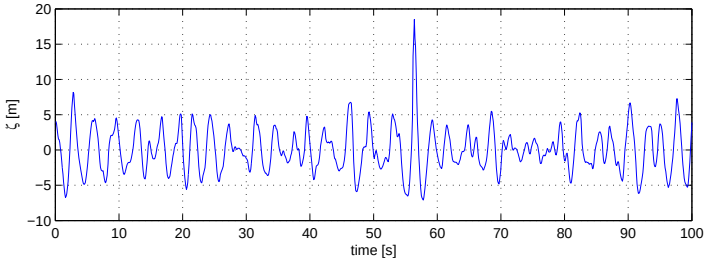

Figure 3: Registration of the surface elevation measured from the Draupner Platform on January 1st 1995, 15:20 GMT. The "New Year Wave" appears at $t = 57$ s (Haver (2000)).

are:

- Seakeeping basin (length $L = 110\ m$, breadth $W = 8\ m$, water depth $d = 1\ m$) of the Technical University Berlin at model scale $1:70$: The spatial development of the "New Year Wave" is measured in a range from 2163 m (full scale) ahead to 1470 m behind the target position by a total of 520 measurements with a resolution of $\Delta x = 0.1\ m$ (see Fig. 4). The optimization approach for the generation of tailored wave sequences with defined characteristics according to Clauss and Schmittner (2005) is used. An analysis of the evolution of the complete wave train is published by Clauss et al. (2008a).

- Large Wave Tank (length $L = 80\ m$, breadth $W = 4\ m$, water depth $d = 1.5\ m$) of the Technical University Berlin at model scale $1:81$: Here, the spatial development of the "New Year Wave" is measured in a range from 1620 m (full scale) ahead to 812 m with a total of 132 wave gauge positions (see Fig. 4). The development and kinematics of this wave train have been investigated in detail by Clauss et al. (2006) and Clauss et al. (2007).

In both cases, the wave breaks shortly after it reaches its maximum crest height. It must be pointed out that although the goal is to generate the same wave sequence the wave board motion is adapted to the respective hydro-electric transfer function of the wave maker, the wave tank characteristics, and the desired location of occurrence. Therefore, the wave board driving signal is generated for each realization separately. (Details are described by Clauss (2008)). The wave contours are shown at the top of Fig. 4 at real world scale. At the bottom of Fig. 4 the time records are shown in comparison - together with the actual measurement provided by Haver (2000). Given the exceptional steepness of the

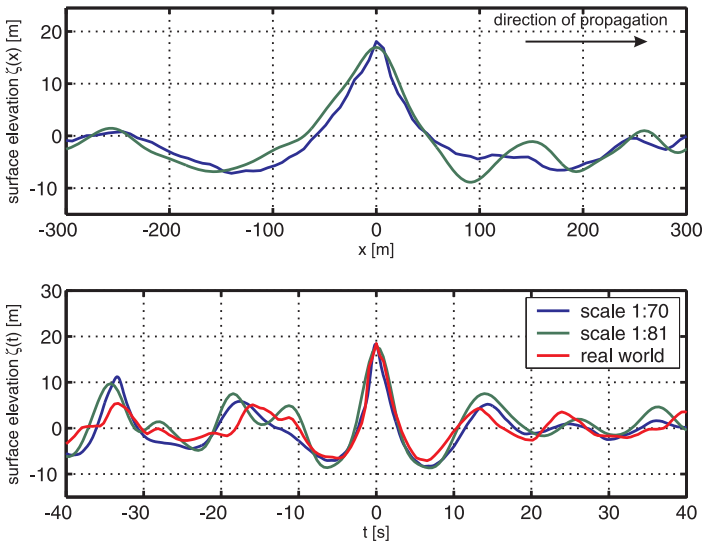

Figure 4: Top: Snapshots of the wave contours of the "New Year Wave" realized in two wave tanks at scale 1:81 and 1:70 (shown in full scale). Bottom: The related time record at the point off occurrence together with the actual real world measurement.

surface elevation a high order wave theory is employed to estimate the underlying kinematics – the Stokes-approximation according to Clauss et al. (2008b). For a given window a velocity profile is approximated by fitting the given surface to the nearest solution of a third order perturbation for sums of interacting Stokes waves according to the formulation by Pierson (1993). Besides the sum of the component waves the solution features higher order terms that are related to all differences and sums of the involved frequencies. The formulation of the free surface consists of the summation of second order Stokes waves, and their interaction terms that are

included up to the third order

$$\zeta(x,t) = \sum_{j=1}^{n} \left(a_j^{(1)} \cos(\theta_j) + a_j^{(2)} \cos(2\theta_j) + a_j^{(3)} \cos(3\theta_j) \right). \quad (6)$$

The index j denotes the component wave while the upper index in brackets denotes the order of the particular term. Altogether, the interaction terms arising from the summation of each frequency pair

$$a_{(1+2)}^{(2)} \cos(\theta_1 + \theta_2) + a_{(1+3)}^{(2)} \cos(\theta_1 + \theta_3) + \ldots + a_{((n-1)+n)}^{(2)}, \quad (7)$$

and the interaction terms arising from the differences

$$a_{(2-1)}^{(2)} \cos(\theta_2 - \theta_1) + a_{(3-1)}^{(2)} \cos(\theta_3 - \theta_1) + \ldots + a_{(n-(n-1))}^{(2)} \quad (8)$$

result in 36 second order terms. Subsequently, interaction terms of third order have the form

$$a_{(1+2+3)}^{(3)} \cos(\theta_1 + \theta_2 + \theta_3) + \ldots + a_{(3-2-1)}^{(3)} \cos(\theta_1 - \theta_2 - \theta_3) + \ldots \quad (9)$$

(a total number of 146). The phase functions are given by

$$\theta_j = k_j t - \omega_j (1+\varepsilon) t + \alpha_j \quad (10)$$

with

$$\varepsilon = \frac{1}{2} \left(\sum_{j=1}^{n} a_j^{(1)} k_j \right)^2. \quad (11)$$

The respective wave potential has a similar form. Its explicit derivation up to the third order is published by Pierson and Moskowitz (1964). The free parameters are the amplitudes $a_{1\ldots n}$, the wave numbers $k_{1\ldots n}$, and the phase shifts $\epsilon_{1\ldots n}$. As indicated in Eq. (10) the waves are assumed to be long crested and propagating along the x-axis. The variation of the parameters is done by a Subplex search algorithm that is applied at each window. The closeness of fit to the real surface defined by the least squares constitutes its objective function.

The resultant magnitude of the horizontal and vertical velocity fields are shown in Fig. 5 where each approximation is scaled to real world for better comparison. The maximum horizontal velocity at the wave tip is 8.05 m/s (scale 1:81, d=125.5 m) and 8.11 m/s (scale 1:70, d=70 m) – almost identical – while the maximum of the vertical component is 4.89 m/s (scale 1:81, d=125.5 m) and 4.62 m/s (scale 1:70, d=70 m) at the preceding zero-upcrossing. The deviation of five percent in the vertical component may also be affected by the slight changes of the instantaneous wave geometry. However, given the overall result shows only small impact of the water depth with regard to the particle kinematics.

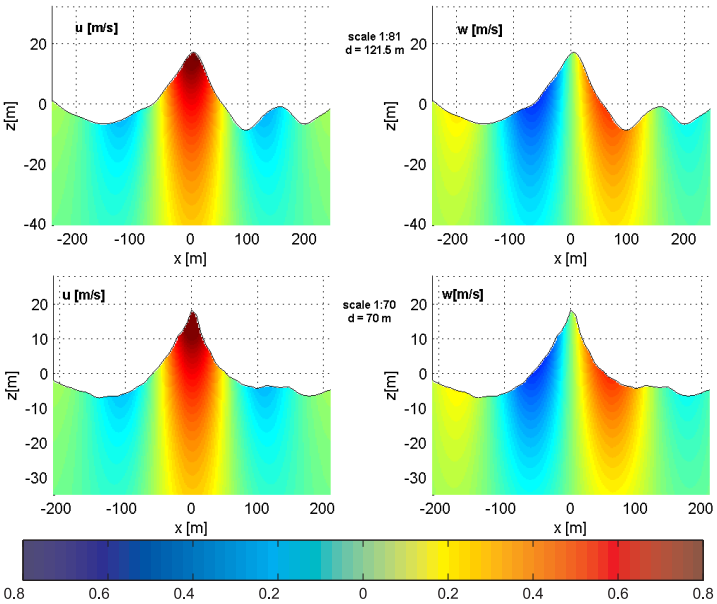

Figure 5: Top: Horizontal (left) and vertical (right) velocity underneath the crest of the "New Year Wave" realized in two wave tanks at scale 1:81 (top) and 1:75 (bottom). Each is shown in full scale.

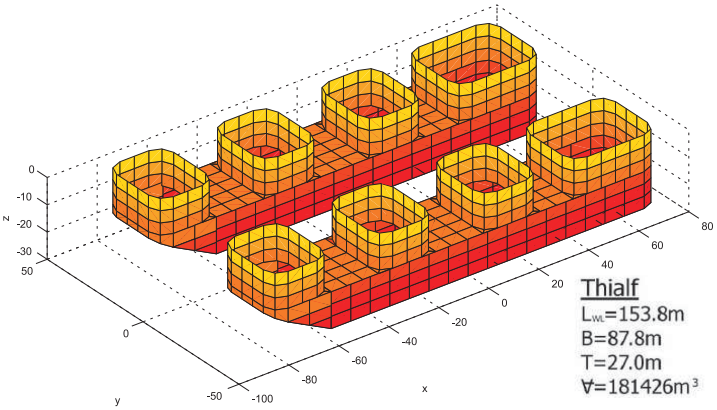

Figure 6: The discretization of the wetted surface of the semi-submersible consisting of 1024 panels.

Having discussed the influence of the water depth on the wave behavior the next section considers the impact of the viable water depth on the wave-structure interaction.

4 MOTION BEHAVIOR OF THE SEMI-SUBMERSIBLE THIALF

With a displacement of about 181,426 tons and a length of the water line $L_{WL} = 153.8$ m the semi-submersible crane vessel "Thialf" (formerly known as DB-102) is one of the largest crane vessels world wide. Its two

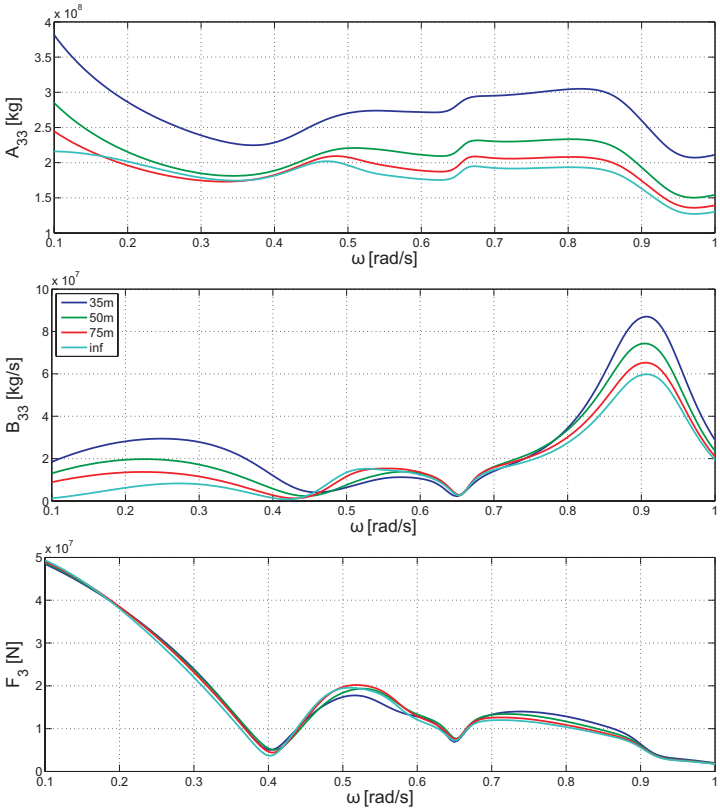

Figure 7: Added mass (top), potential damping (middle), and the exciting force (bottom) coefficients for the heave-motion of the semi-submersible "Thialf" for various water depths.

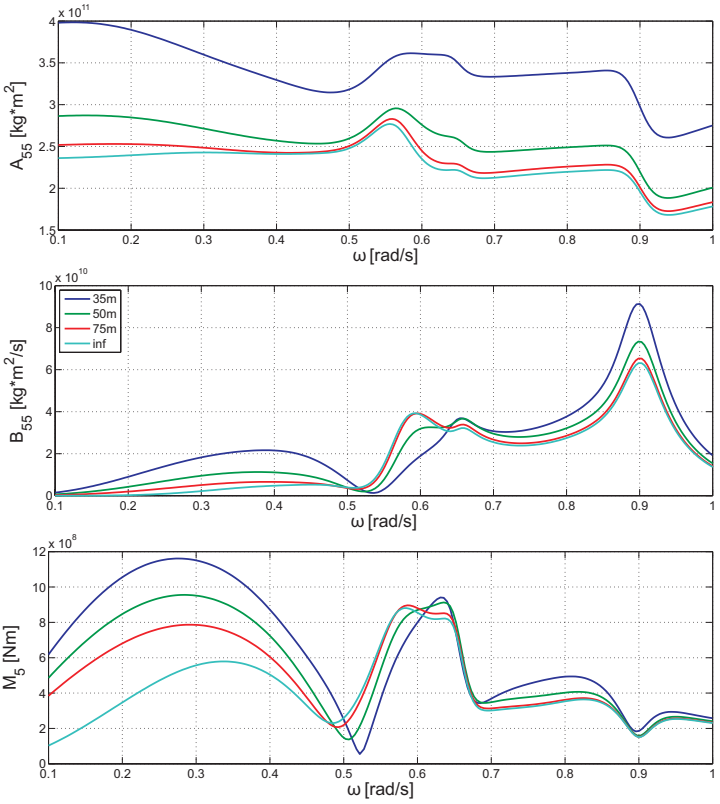

Figure 8: Added mass (top), potential damping (middle) and the exciting momentum (bottom) coefficients for the pitch-motion of the semi-submersible "Thialf" for various water depths.

cranes have a maximum lifting capacity of 14,200 metric tons. It is outfitted with a dynamic positioning system consisting six retractable azimuthing thrusters and 12 flipper delta anchors for station keeping in shallow waters. With its large, deeply submerged displacement (draft: 27 m) it has been chosen for the assessment of the motion response in seaway.

To assess the influence of the water depth on the motion behavior numerical investigations are carried out utilizing the radiation and diffraction code WAMIT (Newman (1977)). In Fig. 6 the discretization of the wetted surface is sketched. In the numerical model the flow potential is divided into the diffraction potential ϕ_7, six radiation potentials $\phi_{1...6}$ (one for each degree of freedom), superimposed with the incident wave potential ϕ_0 (Newman (1977)):

$$\phi = \phi_0 + \phi_{1...6} + \phi_7. \tag{12}$$

The forcing term (shown dimensionally in the direction j) is gained by a pressure integration over the wetted surface S:

$$F_j = \rho \iint_S \frac{\partial(\phi_0 + \phi_7)}{\partial t} n_j \quad ds \tag{13}$$

where n_j is the normal vector pointing out of the structure into the fluid. The matrices of the added mass $\overline{A}$ and potential damping $\overline{B}$ result from the solution of the radiation problem

$$A_{jk} + \frac{iB_{jk}}{\omega} = -\rho \iint_S n_j \varphi_l \quad dS. \tag{14}$$

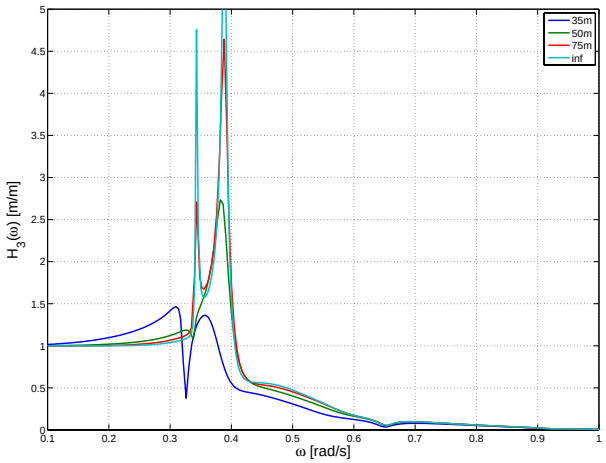

Figure 9: Transfer functions of the heave motion of the semi-submersible "Thialf" calculated with WAMIT showing a frappant change only at $d = 35$ m

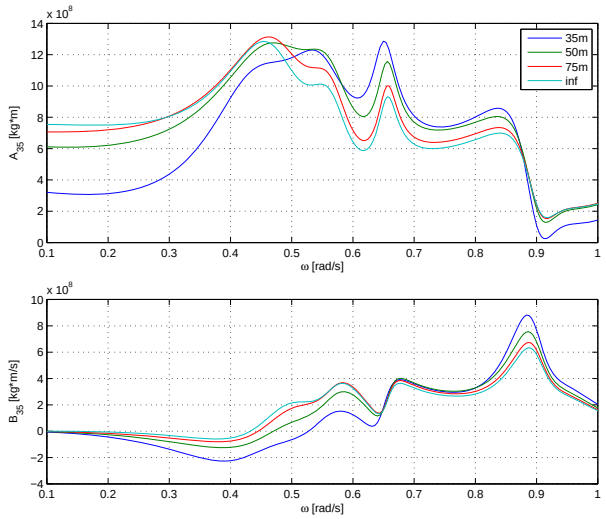

Figure 10: Interaction terms between the heave and the pitch motion showing a change of the sign in the potential damping terms which increases with decreasing water depth.

The matrices have the form:

$$\overline{A} = \begin{bmatrix} A_{11} & 0 & A_{13} & 0 & A_{15} & 0 \\ 0 & A_{22} & 0 & A_{24} & 0 & A_{26} \\ A_{31} & 0 & A_{33} & 0 & A_{35} & 0 \\ 0 & A_{42} & 0 & A_{44} & 0 & A_{46} \\ A_{51} & 0 & A_{53} & 0 & A_{55} & 0 \\ 0 & A_{62} & 0 & A_{64} & 0 & A_{66} \end{bmatrix}$$

$$\overline{B} = \begin{bmatrix} B_{11} & 0 & B_{13} & 0 & B_{15} & 0 \\ 0 & B_{22} & 0 & B_{24} & 0 & B_{26} \\ B_{31} & 0 & B_{33} & 0 & B_{35} & 0 \\ 0 & B_{42} & 0 & B_{44} & 0 & B_{46} \\ B_{51} & 0 & B_{53} & 0 & B_{55} & 0 \\ 0 & B_{62} & 0 & B_{64} & 0 & B_{66} \end{bmatrix}$$

The local potentials φ_l are so called "velocity potential" defined by the identity $\phi_j = \dot{s_j}\varphi_j$ where $\dot{s_j}$ denotes the structure's velocity in j. The matrix of the restoring forces $\overline{C}$ results from the geometry and is defined as:

$$\overline{C} = \begin{bmatrix} 0 & 0 & 0 & 0 & 0 & 0 \\ 0 & 0 & 0 & 0 & 0 & 0 \\ 0 & 0 & C_{33} & 0 & C_{35} & 0 \\ 0 & 0 & 0 & C_{44} & 0 & 0 \\ 0 & 0 & C_{53} & 0 & C_{55} & 0 \\ 0 & 0 & 0 & 0 & 0 & 0 \end{bmatrix}$$

Restoring components from the positioning and anchoring devices are not considered. The motion s is characterized by the following equation of motion in frequency domain

$$\sum_{j=1}^{n} \left[-\omega^2(\overline{M}+\overline{A}) + i\omega\overline{B} + \overline{C}\right] s_j = \overrightarrow{f_j}. \qquad (15)$$

The numerical model allows to examine the impact of the water depth on the left and the right hand side of the equation separately by revealing the hydrodynamic coefficients. The added mass coefficients A_{33} and A_{55}, the potential damping coefficients B_{33} and B_{55}, and the exciting hydrodynamic forces f_3, f_5 are evaluated as shown in Fig. 7 for the heave- and Fig. 8 for the pitch motion. The differences between infinite water depth and $d = 75$ m are marginal. Changes due to smaller water depths appear mainly in the coefficients of the left hand side of the equation of motion (Eq. 15) whereas the forcing terms on the right hand side remains unaffected except for the exciting moments in the low frequency regions which can be explained with the increasing wave steepness. The small variations in the potential damping terms in middle of Figs. 7 and 8 lead to major differences regarding the exact height of the resonance peaks as shown in Fig. 9. This effect is overestimated since it does not yet include the viscous portion of the damping which will be examined in the following. A frappant change of the motion behavior is visible only at the most shallow water depth $d = 35$ m. The two peaks of the resulting transfer functions of the heave motion (Fig. 9) reveal a coupling between pitch and heave motion. It is expressed by the coupling terms related to added mass $A_{35} = A_{53}$ and potential damping $B_{35} = B_{53}$ (shown in Fig. 10) as well as the hydrostatic coefficient $C_{35} = C_{53}$. It is obvious that this effect is sensitive to the water depth and has an impact on the overall motion behavior in the condition of resonance where the restoring and inertial forces cancel each other.

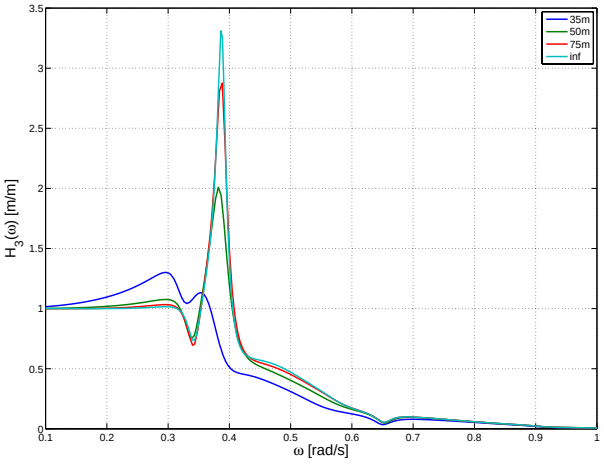

Figure 11: Response Amplitude Operator of the semi-submersible "Thialf" of the heave motion. A viscous damping of $\approx$ 1.2 per cent of the critical damping is assumed.

5 VISCOSITY

The influence of viscous damping is not covered by WAMIT but it has crucial influence on the motion

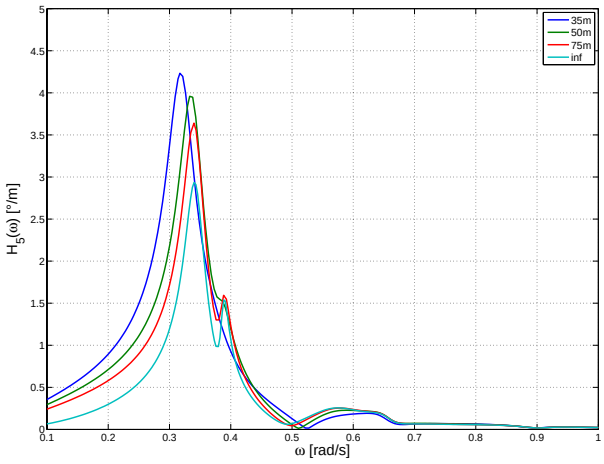

Figure 12: Response Amplitude Operators of the semi-submersible "Thialf" of the pitch motion. A viscous damping of ≈ 2 per cent of the critical damping is assumed.

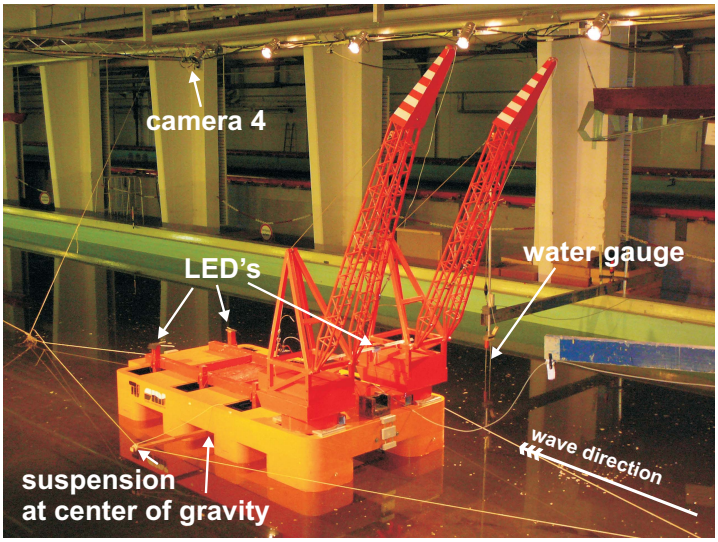

Figure 13: Experimental setup to determine the transfer functions of the pitch and heave motion of the semi-submersible "Thialf" (scale 1:75).

behavior in the resonant frequency band. It has been derived experimentally from the logarithmic decrement in resonance tests and is estimated to be 1.2 per cent of the critical damping in heave and 2 per cent for the pitch motion. These viscous effects are added to the respective coefficients in the damping matrices. Fig. 11 and 12 show the resulting response amplitude operators for each water depth taking into account the viscous terms. It becomes obvious that the addition of the viscous effects changes the motion behavior by eliminating the low frequent peak of the heave response amplitude operator which is attributed to the heave-pitch coupling.

6 MODEL TESTS

In parallel the motion behavior of the semi-submersible is analyzed experimentally by model tests at scale 1:75 at various water depths. The experimental setup to determine the transfer functions is shown in Fig. 13. The suspension allows free pitch and heave motions while all other degrees of freedom are slightly restrained by a soft spring-counterweight mooring system. The transfer functions are gathered using transient wave packages – affirmed by tests in regular waves (for details see Clauss (2008)). The results of the experiments for heave and

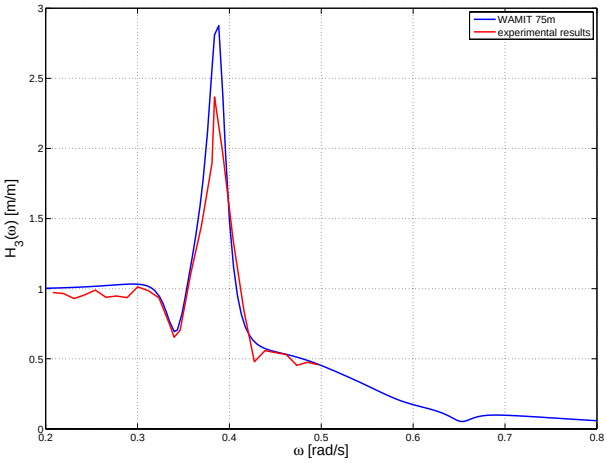

Figure 14: Response amplitude operators for heave motion of the semi-submersible "Thialf" at water depth $d = 75$ m. The comparison shows good agreement between experiment and WAMIT.

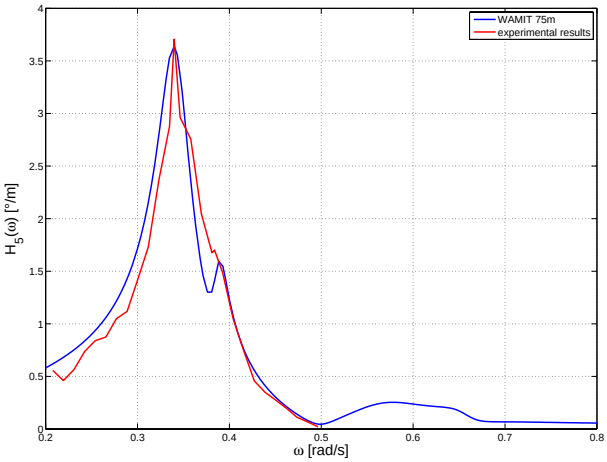

Figure 15: Response amplitude operators for pitch motion of the semi-submersible "Thialf" at water depth $d = 75$ m. The comparison shows good agreement between experiment and WAMIT.

pitch motions are shown in Figs. 14 and 15 in comparison with the respective numerical results (including viscous damping).

7 DISCUSSION AND CONCLUSIONS

The deterministic wave sequence – the New Year Wave – is presented being realized in two wave tanks at $d = 70$ m (scale 1:70) and at $d = 121.5$ m (scale 1:81). The generation signal is customized to the particular wave tank in such a way that identical wave contours are obtained. Although the relative water depth differs significantly the particle kinematics close to the surface in the wave crest region show very alike behavior.

Looking at the seakeeping study (with Fig. 2 in mind) it is not surprising that the exciting heave forces on the semi-submersible remain virtually unaffected when the water depth is reduced from infinite to $d = 75$ m, and only small changes occur when d is further reduced to 50 m (see bottom of Figs. 7 and 8). The exciting pitch moments show strong deviation only at the low frequency region – an effect that is attributed the wave steepening effect due to the dispersion relation (Eq. 3). Moderate changes in the response amplitude operators occur due to the water depth dependency of the damping and added mass coefficients. Only in the case of most shallow water $d = 35$ m a fundamental change of the motion behavior is observed due to the massive increase of the added mass and potential damping (see Fig. 7 and 8) as well as a strong coupling as shown in Fig. 10. It is obvious that the water depth influences mainly the left hand side of the equation of motion (Eq. 15) at $d \leq 50$ m whereas the forcing remains constant even in shallow waters (providing that the wave steepness remains constant). The comparison with the results in deep water and the agreement with the model test results (Fig. 14 and 15) indicate that the water depth of 75 m (or ≈ 1 m at model scale) is sufficient to carry out model tests with free floating structures where deep water is assumed.

ACKNOWLEDGEMENT

This paper is published as a contribution to the project HANDLING WAVES, which is funded by the European Commission, under the contract TST5-CT-2006-031489. We highly acknowledge the support of this research project. The authors also wish to thank Mr. Lucas Montagne for his valuable preliminary studies on the matter.

REFERENCES

Clauss, G. (2008). The Taming of the Shrew: Tailoring Freak Wave Sequences for Seakeeping Tests. *Journal of Ship Research*, 52:194–226.

Clauss, G., Klein, M., and Testa, D. (2008a). Spatial Evolution of an Extreme Sea State with an Embedded Rogue Wave. In *OMAE 2008 - 27th International Conference on Offshore Mechanics and Arctic Engineering*, Estoril, Portugal. OMAE2008-57229.

Clauss, G., Stempinski, F., and Klein, M. (2007). Experimental and Numerical Analysis of Steep Wave Groups. In *12th IMAM - International Congress of the International Maritime Association of the Mediterranean*, Varna, Bulgaria.

Clauss, G., Stempinski, F., and Stück, R. (2008b). On Modelling Kinematics of Steep Irregular Seaway and Freak Waves. In *OMAE 2008 - 27th International Conference on Offshore Mechanics and Arctic Engineering*, Estoril, Portugal. OMAE2008-57228.

Clauss, G., Stück, R., Stempinski, F., and Schmittner, C. (2006). Computational and Experimental Simulation of Nonbreaking and Breaking Waves for the Investigation of Structural Loads and Motions. In *25th International Conference on Offshore Mechanics and Arctic Engineering (OMAE)*, pages 1–9, Hamburg, Germany.

Clauss, G. F., Lehmann, E., and Östergaard, C. (1992). *Offshore Structures*, volume 1: Conceptual Design and Hydrodynamics. Springer Verlag London.

Clauss, G. F. and Schmittner, C. E. (2005). Experimental Optimization of Extreme Wave Sequences for the Determinsitic Analysis of Wave/Structure Interaction. In *OMAE 2005 - 24th International Conference on Offshore Mechanics and Arctic Engineering*, Halkidiki, Greece. OMAE2005-67049.

Haver, S. (2000). Some Evidences of the Existence of so-called Freak Waves. In *Rogue Waves 2000*, Brest, France.

Jacobsen, K. and Clauss, G. (2005). Multi-body Systems in Waves and Impact of Hydrodynamic Coupling on Motions. In 12th *International Congress of the International Maritime Association of the Mediterranean (IMAM)*, Lisboa, Portugal.

Newman, J. (1977). *Marine Hydrodynamics*. The MIT Press, Cambridge, Massachusetts.

Pierson, W., J. (1993). Oscillatory Third-Order Perturbation Solutions for Sums of Interacting Long-Crested Stokes Waves on Deep Water. *Journal of Ship Research*, 37(4):354–383.

Pierson, W. J. and Moskowitz, L. (1964). A Proposed Spectral Form for Fully Developed Wind Seas Based on the Similarity of S. A. Kitagorodskii. *Journal of Geophysical Research*, 96(2).

Riekert, T. (1992). *Die Dynamik von Schwimmkranen mit hängender Last*. PhD thesis, Technische Universität Berlin (D 83), ISBN 3-89249-140-2, Verlag René F. Wilfer, Spardorf.